IEEE Access
Multidisciplinary ⋮ Rapid Review ⋮ Open Access Journal

Received 18 October 2024, accepted 3 November 2024, date of publication 8 November 2024, date of current version 18 November 2024.

Digital Object Identifier 10.1109/ACCESS.2024.3494055

RESEARCH ARTICLE

Intelligent Residual Current Monitor Application in Hospital With Fiber Optics Using Wavelength Division Multiplexing

ERWIN SUTANTO[1,2], (Graduate Student Member, IEEE), GUILLERMO ESCRIVÁ-ESCRIVÁ[3], SAMIAN SAMIAN[4], HENDRA KUSUMA[1], (Member, IEEE), AND TRI ARIEF SARDJONO[5], (Member, IEEE)

[1]Department of Electrical Engineering, Institut Teknologi Sepuluh Nopember, Surabaya 60111, Indonesia
[2]Biomedical Engineering Department, Universitas Airlangga, Surabaya 60115, Indonesia
[3]Institute for Energy Engineering, Universitat Politècnica de València, 46071 Valencia, Spain
[4]Department of Physics, Universitas Airlangga, Surabaya 60115, Indonesia
[5]Department of Biomedical Engineering, Institut Teknologi Sepuluh Nopember, Surabaya 60111, Indonesia

Corresponding authors: Erwin Sutanto (erwin_sutanto@fst.unair.ac.id) and Hendra Kusuma (hendraks@ee.its.ac.id)

This work was supported by Airlangga Research Fund 2024 from Universitas Airlangga under Contract 435/UN3.LPPM/PT.01.03/2024.

ABSTRACT In this study, we propose the implementation of integrated leakage current detection in residual current monitor (RCM) to control safety protection in microgrid-based hospitals. Using memory-based features to magnify statistical significance, we tried different sampling periods to build a classification model from a sample of RCD induction voltage dataset using support vector regression (SVR). The model was then tested by individually comparing sampling lengths from 2 to 16. The proposed method can also achieve fast and valid detection according to the signal pattern within 5.45ms for H-L sequence with H;high and L;low. By adding the time series method using long short-term memory (LSTM), the detection speed could be further confirmed using H-L-H sequence with root mean square error (RMSE) around 1.% The use of Fiber Optics (FO) can also ensure coordinated control of the microgrid. The detection system can be carried out without delay by separating the machine learning at the server and the digital residual current device (RCD). The digital RCD was synthesized using a Xilinx field-programmable gate array (FPGA) based on XC6SLX16-2FTG256C. The proposed method uses only 184 Registers and 1,656 lookup tables (LUTs). The results present the classification using a designed digital RCD to detect possible leakage current condition (LCC), data delivery to the server via FO using wavelength division multiplexer (WDM), and LSTM acceleration to support the microgrid protection system. This new approach will help develop load fault protection via FO to maximize communication speed, and improve patient safety by localizing the potential hazards.

INDEX TERMS Smart microgrid, residual current monitor, medical devices, protection, affordable and clean energy.

I. INTRODUCTION

Microgrid in hospitals generally uses distributed energy resources (DER) to increase the resilience of electricity supply when power outages occur as a result of the large number of medical devices commonly seen from the single line diagram (SLD) [1]. This includes the use of distributed generations (DG) connected to distributed energy resources (DER) as an alternative renewable energy source (RES) in the microgrid system using a control and energy management system (EMS), using energy storage (ES) as a buffer between the two so that the load supply can be controlled with negotiation protocols with relay coordination [2]. These conditions require data analysis and determination of

The associate editor coordinating the review of this manuscript and approving it for publication was Qiang Li.

threshold values as limit parameters from power conditions and in terms of protection and power efficiency [3]. Analysis of leakage currents on loads in electricity distribution can be useful for managing electricity supply and planning the supply duration to loads when power outages occur by disconnecting loads that have a high probability of being in leakage current condition (LCC). The development of integrated leakage current detection in the residual current monitor (RCM) for safety protection control as the main function and ground fault diagnosis is an ongoing work with this research with improvements in terms of speed using fiber optics (FO) [4]. The black start service is essential in the emergency hospital operating landscape. Therefore, significant adjustments are needed to enable the involvement of limited alternative energy sources, especially RES units such as Photovoltaic (PV) Arrays, or aggregated units such as offshore wind power plants (WPP) if necessary [5].

The use of locally generated electricity from sources such as generators, wind turbines, PV Arrays, and batteries require real-time monitoring and dynamic control due to its independent nature. This monitoring will ensure reliable and safe operation with the use of FO [6]. Likewise, the electrical load in modern hospitals that use modern medical equipment is not only increasing in terms of quantity but also variety. Therefore, technically residual current measurements need to be carried out as well as one of the requirements for the safety standards of medical devices against the dangers of electrical shocks [7]. The condition of the supply disconnection for reasons of protection must also take into account the occurrence of errors if the method of analyzing the shape of the leakage current signal is not used according to normal conditions (NC) and single fault condition (SFC) of the load. This will ensure that false alarms occur as little as possible and still ensure that the microgrid is in a safe condition so that there is no potential for nuisance trips [8].

On the other hand, Artificial Intelligence (AI) has developed and become popular recently because of its ability to overcome complex interactions as an advantage in analyzing electrical safety with various computations with large and diverse data sets [9], [10], [11], [12], [13] but not much about detection time. Where the use of machine learning methods are also utilized, such as; time series analysis and various regression and classification techniques such as support vector machine (SVM) [14], [15], Artificial Neural Networks (ANN) [16], and reinforcement learning (RL) [17] to predict in the form of probability. However, the disadvantage of the application was not for fast protection. These techniques use sophisticated learning mechanisms and computational algorithms to obtain in-depth information from recorded data. Deep learning techniques have been proven to perform very well in various fields and have many advantages with the ability to predict from historical data [18]. This is before the possibility of undetected trips outside the fundamental frequency as most RCDs are based on rated residual current, I_{Δ} [19]. The fast safety response vs. confirmed trips is still a novelty.

As comparisons of the proposed residual current-based system, some common methods could be used. One typical method is generally done by diagnosing any changes in residual current on the distribution to distinguish from NC with a threshold. However, this kind of detection can also be mistaken by any switching [20], such as; capacitor switching, or generator switching in a microgrid system. This weakness could be fixed by using machine learning as discussed. It is by updating the weight coefficients of the model as configurable thresholds. This method has been proposed to fill the gap between real and expected variables [21].

There is also a possible residual current scenario in different measurements used for the diagnosis process [22]. In the microgrid case, the inverter current might be influenced by its operating mode and various loads in the same distribution [23]. In this hospital perspective, any current loss that would be detected by RCD could come from various currents, such as leakage current on medical devices, touch current on patients or operators, or fault current in the power distribution. The condition would be referred to as the LCC.

This work proposes a hybrid diagnostic scheme to combine a faster protection strategy with a digital residual current device (RCD) directly at the load point and the use of a server with greater computing power as its contributions to add microgrid fault protection with patient safety parameter. This will make it effective in guarding against potential leakage current hazards directly at the site and keeping its threshold value updated based on features from support vector regression (SVR) machine learning and time series with long short-term memory (LSTM) method to accelerate the detection via FO communication as a speed novelty. Furthermore, this paper is organized in the following order. An example of a microgrid system and the coordination of relay protection faced is described in section II. A detailed analysis of the feature technique of machine learning with the SVR method and the results of various test cases are provided such as LSTM and the design of the proposed digital RCD is in section III. Including, the FO signal testing using wavelength division multiplexer (WDM) technique for an efficient communication system between digital RCD and server, and the synthesis results with Xilinx field-programmable gate array (FPGA) based on Spartan-6 Core, XC6SLX16-2FTG256C in the last subsection III-C. The comparison of this method with others would be in III-D and concluded in section IV.

II. METHODS

Early detection of signals from the load with residual current measurements to ensure the safety of the microgrid and electrical efficiency is the main objective of this study. The leakage current measurement instrument is then made by prioritizing the achievement of electrical safety standards. The safety of hospital patients will be determined by analyzing the amount of leakage current and its duration. One of the ways is by ensuring the sequence of leakage current signals in a general microgrid diagram.

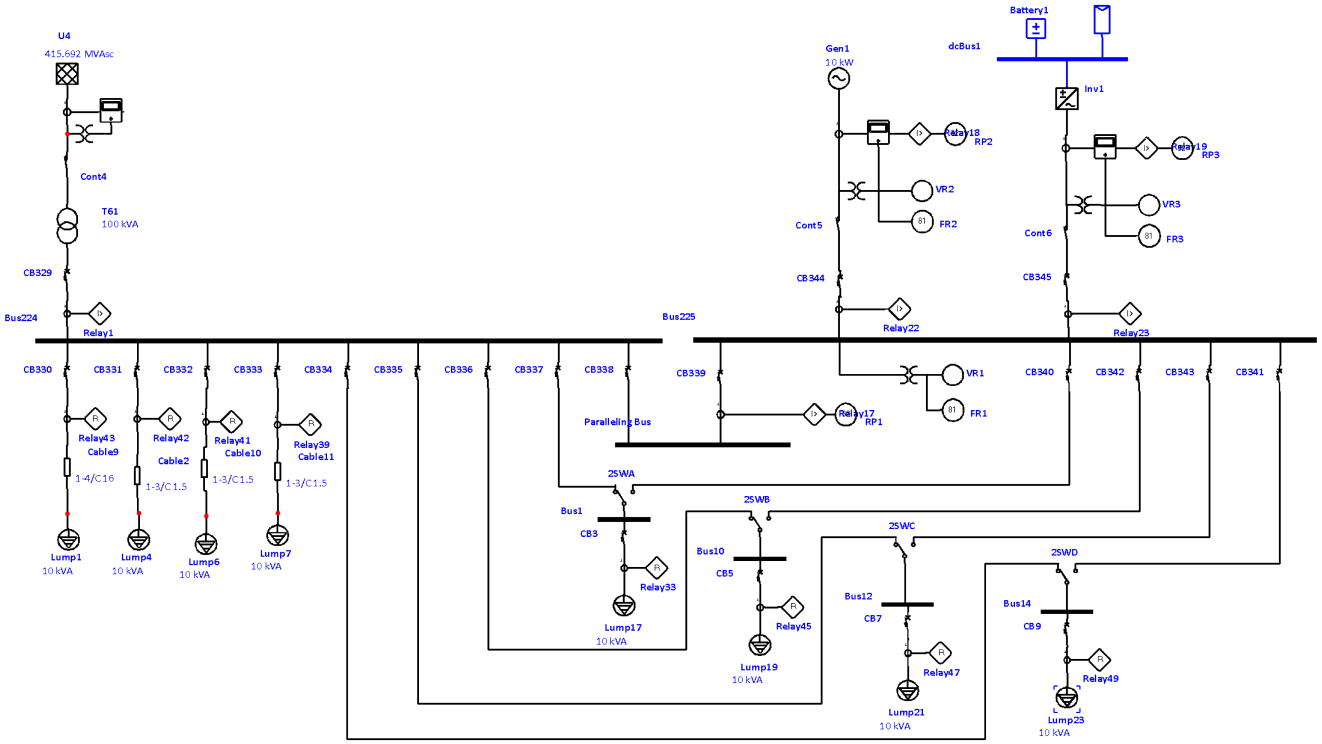

FIGURE 1. Example of on-site paralleled energy resources in hospitals.

A. RESIDUAL CURRENT MONITORING (RCM) AND ITS POSSIBLE SPEED

The single line diagram in Fig. 1 is an example of a microgrid showing the implementation of a paralleled emergency generator system on site to reduce the peak utility load demand and supply for black start services for health care facilities. This is necessary to ensure load balancing between supply and demand for the energy and ensure uninterrupted conditions in the operating room in an emergency framework. This grid facilitates active energy sources from the main power grid, U4 with alternative sources with RES such as PV arrays and batteries in a DC Bus, dcbus1, before going to the Inverter, Inv1. Likewise, DG, Gen1 as the main alternative in supplying when U4 is off, the distribution load network of medical equipment can still be served. Life support in the intensive care unit (ICU), baby incubators in the neonatal intensive care unit (NICU), and electrosurgical equipment in the Operating room (OR) are part of the general load in the hospital. These various loads could be seen as an example of network loads Lump1-Lump7 which are divided into the distribution of circuit breakers (CBs), namely, CB330-CB343.

Early detection of electrical faults from the residual value side will help in minimizing the energy expenditure of the hospital. Residual current detection methods are also commonly used and have been discussed both from the machine part such as permanent magnet synchronous motors (PMSMs) [22], [23]. However, it may not be general to electricity diagnosis. Effective energy usage and load balancing are some of the benefits that can be obtained by the observation method in microgrid. Apart from its specific function in hospitals to consider the hazard protection factor for patients in their activities with all the medical equipment that has been mentioned one by one. Consideration of control functions in microgrid becomes more complicated [24]. These functions include the ability to switch modes from the main grid to island mode with inverters, and the utilization of DG to black start services as shown in Fig. 1 if there is a power outage in the main grid. Some parameters of fault detection using residual methods are discussed in Table 1.

TABLE 1. Fault detection using residual methods.

No	Parameter	Hosseini et al., 2020 [2]	Wang et al., 2021 [21]	Biswal and Parida, 2022 [20]	Sutanto et al., 2024 [4]
1	Adaptive threshold	Yes	Yes	Yes	No
2	Time duration	Yes	Yes	No	Yes
3	Relay speed	Yes	No	Yes	Yes

Table 1 shows that three parameters can be analyzed as an approach to four references with the Residual method in Fault Detection. The first parameter is the adaptive threshold. Conditions in islanded mode compared to normal mode, show a reduced total fault current so the relay threshold setting also needs to follow to be lower [2]. Changes in the threshold value are also recorded as needing to change according to the diagnostic value of the eigenvector modulus, eigenvector

angle, and the magnitude of the neutral point potential [21]. Furthermore, threshold determination can use vector path prediction although this diagnostic technique is intended for a T-type inverter system with four wires. Reference [20] is more intended for detecting high impedance fault (HIF). Also, the need for changes in the threshold value with a value of zero for normal mode and more than zero when HIF occurs. Only [4] does not record changes in the threshold and uses the control value on the relay at a value. If there is no fault, the leakage current is still within the tolerance value.

The second parameter is Time duration. Delay is the protection time that is delayed from the initial detection of a fault indication to its resolution. Here, the variable $t_{detection}$ is the detection time while $t_{coordination}$ is the time for Relay coordination from each point in the system. Finally, $t_{communication}$ is the latency time of communication from associated links [2].

$$t_{protection} = t_{detection} + \sum t_{coordination} + t_{communication} \tag{1}$$

There are several methods to shorten the diagnosis time, namely by providing temporary defect information by detecting it hardware-wise in the inverter [21]. New fault detection can be communicated in several transition cycles from the relay coordination stage, $t_{coordination}$. Reference [20] does not really define it in time because the method is to utilize frequency as a time comparison. The method used is to use residual voltage in continuous wavelet transforms (CWT) analysis with a sampling frequency of 4 kHz. Time-frequency analysis of residual voltage allows fault differentiation, namely by identifying the power frequency band. Reference [4] uses the time difference between the response to the step signal and the peak voltage of the impulse signal, each of which is different from the other.

Finally, the Relay speed parameter depends on the communication protocol used. Reference [2] uses RS232 to coordinate a pair of relays with a predetermined delay time. Reference [21] does not discuss the timing issue. Depending on the device's status, the current route in the inverter will be set during normal operation. While [20], looking at the properties of the HIF feature, the relay will be triggered under balanced loading conditions. Reference [4] uses IoT to help find potential sources of fault current leakage effectively and activate multilevel relay protection in microgrid power distribution. IoT can then confirm the detection of ground fault current by recording the potential trip value at each monitored load point.

In microgrid, connection changes due to DG transfer or load disconnection can occur. Load-sharing techniques, control, and additional protection strategies that will be applied to realize all of this often become erroneous due to these changes [25]. For this reason, an additional digital tool is needed to assist the microgrid control system. Relays that have been commonly used require communication to determine the source of the fault current, adjust the operating

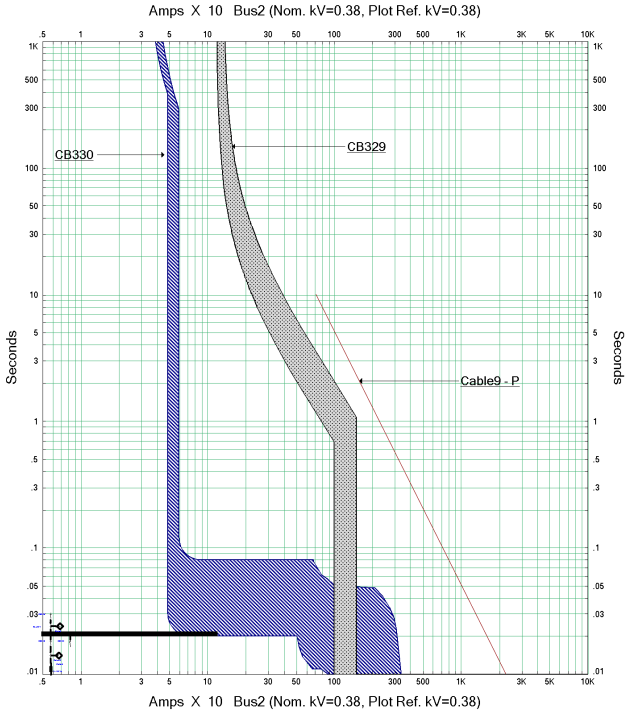

FIGURE 2. Ampere vs time Chart of the protection coordination.

current conditions, and isolate the fault properly. With additional information on the source of the fault quickly, the burden on the microgrid central protection unit (MCPU) in tracking the status of each DG or load will be lighter and focus on its control function.

One of the classic problems of limited and nonlinear optimization is the classification of directional overcurrent coordination relays (DOCR). Where the relay used is not only seen from its function as a protection relay against the load but also requires certainty with the backup relay. As the name implies, the backup relay must function after a specified time interval if the primary relay fails [26]. We call it relay coordination. Relay coordination must be done correctly so we can depend on the protection mechanism. Therefore, choosing the correct plug setting (PS) and time setting multiplier (TMS) is crucial for proper relay coordination. The calculation of the general time duration is formulated in (2).

$$t_{relay} = \frac{\beta}{(\mathrm{PSM})^{\alpha} - 1} \times \mathrm{TMS} \tag{2}$$

PSM is multiple PS and constants α and β are slope values that vary depending on the time-current curve aspect of an overcurrent relay (OCR), as shown in the curve Fig. 2. Finding the optimal values of PS and TMS in an integrated power system is a challenging problem [27]. An optimization approach can be used to find the optimal selection of PS and

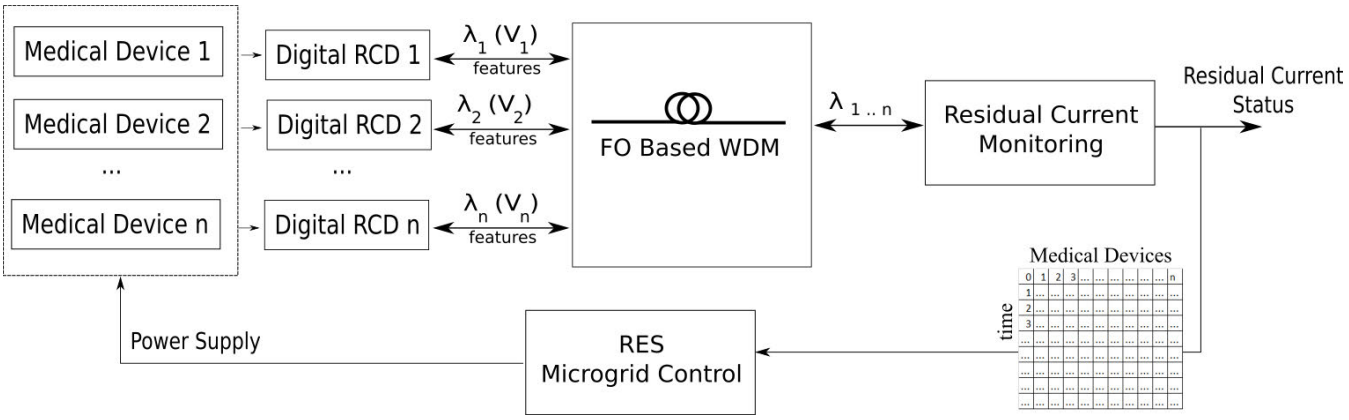

FIGURE 3. Block diagram with fiber optics using wavelength division multiplexing.

TMS with the objective function (3) as shown below;

$$OF = \min \sum_{i=1}^{N} t_{relay}\,(i, j) \tag{3}$$

N is the total relays in the network, and $t_{relay}\,(i, j)$ is the operating time of the relay with index i when a fault of j occurs. The main disadvantage of this objective function (OF) is that it only minimizes the working time of the primary relay without taking into account that the increase allows a longer time difference between the primary relay and the backup relay.

Figure 2 shows the relay for time protection coordination for possible over different current values of CB329, CB330, and cable9. Everything needs to be coordinated when a current fault occurs in the Lump1 load in Fig. 1. The coordination limits protect against accidental or uncoordinated tripping of the relays and ensure that the load relay at CB330 and the backup relay function properly. The operating period of the backup relay at CB329 must exceed the operating time of the load relay by a predetermined amount in the coordination time interval (CTI) to ensure correct $t_{coordination}$ [27].

$$t_{backup} - t_{load} \geq t^{\min}_{coordination} \tag{4}$$

The traditional technique for detecting leakage current in securing the electrical network is by measuring the magnitude of the leakage current using an RCD. The problem faced is the existence of false trips due to the generally assumed leakage current limit value. However, in principle, if leakage current detection cannot distinguish between leakage current under normal conditions and leakage current that can cause interference, the classic RCD can no longer detect interference reliably [28]. This condition is further complicated by the absence of a guarantee that normal conditions with noise in the form of electrical impulses do not cause the same RCD trip as when leakage current occurs, known as nuisance trips [8]. The Detection here is faced with three challenge parameters that were discussed previously. Due to this, the digital type of RCD on the load side and the use of a server on the central side with computing power will be the solution.

Figure 3 shows the block diagram of the proposed system that relies on FO communication media with transmission speeds that minimize $t_{communication}$. By using IoT [4], signals can be sent from anywhere without the need for rigid settings but are hampered by transmission speeds from the patient's safety side, especially for leakage current values above 20mA. The solution for this speed is with FO where communication time becomes more tolerant but is comparable to the cost efficiency for FO installation. The use of FO requires many labor installation rules because FO is made of glass so it is fragile, cables can break or lose signal if bent or curved in a few millimeters.

Figure 3 also combines the use of microgrid control with relay coordination and RCD detection for load protection as well as fast speed communication as discussed in [29]. Basically, the Mux device in the WDM system combines several N data channels that will come from several local RCDs before being sent through the FO. The Demux will receive signals in the form of light and divide them according to their respective wavelengths. This also allows more advanced processing with optical processors, which have been produced from various structures [30]. As a start, the presentation of the possibility of a neuron architecture that combines coherent optics with WDM and towards a neural network platform based on FO with RCDs as its fault source. Here, the use of WDM to enrich the combination of power distribution with parallelization capabilities throughout the fan-in stage and weighting transfer to serve the purpose of centralized computing. In this case, each signal is then evaluated by the receiver, which will activate the backup relay or CB associated so that it can isolate the faulty area to a certain extent.

The concept used is the total current flowing through the RCD under normal conditions is close to zero. On the contrary, when an electrical shock occurs as shown by the following expression where I_{LL_1}, I_{LL_2}, to I_{LL_N} are the currents lost from the Lump1, Lump4, and Lump-N in Fig. 1.

TABLE 2. Disconnection time over different leakage current values.

Current	Let-Go Time
5 mA	10 s
10 mA	2 s
20 mA	500 ms
50 mA	100 ms
200 mA	10 ms

Respectively, I_{LL} is the total leakage current from lumped loads:

$$I_{LL_1} + I_{LL_2} + \ldots + I_{LL_N} = I_{LL} \tag{5}$$

FO as a technology used to transfer data from one end of the circuit to another has been widely used in various applications including protection [31]. Light pulses are used in this system as data signals. In comparison, copper cables are not used in situations that require long distances, because of their relationship to the need for high-speed data transfer or wide bandwidth on the contrary [31]. It is in accordance with the detection of the risk of electric current surges that may occur due to various reasons. From a safety perspective, if there is a current of more than 200mA on a single phase 220V that hits the patient for more than 10ms, this will exceed the patient's ability to escape from the shock and will be at risk of further danger. The disconnection time guideline for the longest duration per voltage range to prevent electric shock accidents is shown in Table 2. As suggested by [32], the electric current is disconnected when the patient starts to feel the electric shock at the threshold of the perception stage to avoid a riskier stage. The most important aspect of a microgrid system in a hospital is safety. Periodic enhancement of the protection and control system needs to be done considering the increasing demand and continued utilization of RES. This residual current approach can be used to support the fault diagnosis standard in the relay system discussed earlier.

Table 2 follows the International Electro-technical Commission (IEC) standard for medical devices in IEC60601 [33]. The Let-Go Time can be used as a reference for the permissible exposure time. The microgrid control system has a major impact on how it works in adopting the standard. With the proposed mechanism, the microgrid control can focus on maintaining stability and allow it to adjust its operating point without exceeding the previously set operating limits, as mentioned in IEC 61850 [34]. With the use of WDM, one communication path can be utilized to monitor multiple loads in adjacent locations. The proposed WDM network will meet the minimum basic efficiency requirements regardless of changes in bit rate or possible $t_{communication}$ [35]. As an illustration, an 8-channel WDM optical communication system with a data rate of 40 Gbps has been designed with a distance of 10,000 km [36]. Another study with only a passive optical network (PON) suggested that the application was within a 1 km distance with a frequency of 10 GHz [29]. Both studies show its potential for being used in a large area. WDM basically can be combined into a wider network, by utilizing one path at a certain wavelength with N receivers operating n wavelengths according to the number of load distributions in a unique microgrid distribution system with various nodes. Then, all transmitter outputs are sent to the receiver evenly and passively using a star topology [37].

B. DATA SEQUENCE LEARNING

Status detection is highly dependent on $t_{detection}$ given previously in (1). This is the most important factor to speed up the protection time. The status value will be used directly for the power supply switch in the medical device using RCD. Therefore, the result of detection at this stage can eliminate unconfirmed predictions as much as possible. In this way, patient safety can be achieved according to IEC standards. To eliminate false signals, the residual current signal pattern approach could be used.

Figure 4 displays an example of the signal using the digital RCD which is shown later at Fig. 7 from a 7W load with a 220V AC supply voltage with a frequency of 50 Hz. A load with a larger wattage will allow for a higher voltage rating. The dataset could be accessed at [38]. The signal is obtained by turning on the load for around 0.035 seconds at NC, before simulating the SFC as shown in Fig. 4 with status; 0 for NC, and then followed by the SFC status; 1 for LCC. Signals with arbitrary waveforms can be measured and characterized by digital sampling system such as in electrocardiogram (ECG) [39]. Similarly, the signal for the LCC is formed with a periodic wave pattern according to the power source.

$$T = \frac{2\pi}{\omega} \tag{6}$$

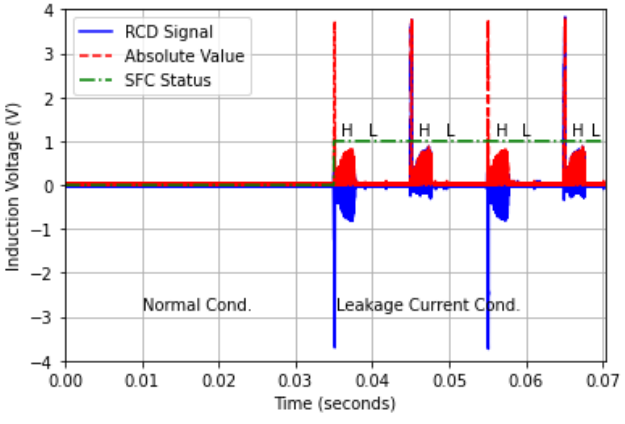

FIGURE 4. Sample of RCD induction voltage.

When T is the period value of the signal and ω is obtained from the frequency value of the power supply, it will be found that the value of T is 20ms. Thus, one supply wave is formed by two patterns using the absolute value of the RCD signal which are shown in red in Fig. 4. In each of these patterns as seen in the figure, there are two groups of values, namely; high value (H) and low value (L). Where H begins with a peak

in the form of an impulse, as follows;

$$\delta_H[n] = \begin{cases} 0 & \text{if } n \neq I, \\ Peak & \text{if } n = I. \end{cases} \tag{7}$$

With the value of I approaching zero, the impulse value is the peak value commonly used to deactivate the relay on analog RCD. However, the interphase current reaches a higher peak value depending on the voltage in each phase and at certain times exceeds the residual current standard, I_Δ. These peak numbers can trigger trips [8]. On the other hand, this value is basically the earliest value to detect the presence of leakage current. The next stage is the pulse signal with high frequency, as follows;

$$\chi_H[n] = \begin{cases} f[n] & \text{if } n \in P \\ 0 & \text{if } n \notin P \end{cases} \tag{8}$$

With the same characteristic value as before, (8) has a lower Amplitude value compared to the peak value of the initial stage of H. P is defined in the period of the pulse with high frequency, f[n] before entering the last stage, L with a value approaching zero as in normal conditions. With this signal pattern, detection H part of LCC can use these two characteristics as in I and P as a more accurate determinant compared with just the peak value as in most analog RCDs.

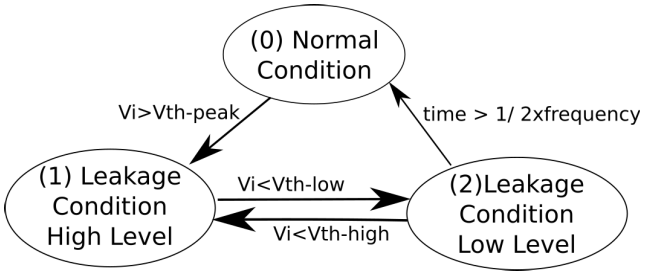

FIGURE 5. Control flow graph.

Figure 5 shows the possible control flow graph (CFG) of the repetitive H-L pattern with 3 states of finite-state machine (FSM). In this study, we try to design the detection with a simple digital RCD using FPGA to realize the CFG. The combination of peak and amplitude values will be studied with machine learning in several features. The next stage for prediction with the entire signal pattern will be carried out on the Server which also functions as a residual current monitor (RCM) which will also monitor the values obtained in the digital RCD as seen in Fig. 3 previously.

$$V_{Induction} \in \mathbb{R}^D \tag{9}$$

$$\phi : \mathbb{R}^D \rightarrow \mathbb{R}^M, \phi(V[n]) \in \mathbb{R}^D \tag{10}$$

Induction voltage $V_{Induction}$ data is read using ADC from analog RCD. The data is then mapped to $\mathbb{R}^D$ in a memory buffer to utilize the sampling rate read from the ADC chip and controlled directly by FPGA. The LCC will be classified in the conversion at the input $\phi(V[n])$. From this classification function, the control will then be determined as described in the CFG in Fig. 5. Based on the threshold value V_{th} with three values, they are; $V_{th-peak}$, $V_{th-high}$, and V_{th-low}.

$$\mathcal{H} : z = w.\phi + b \tag{11}$$

Equation (11) shows the linear equation of the model to be formed with y as the space for detection status, w as the load for each ϕ and b as a constant value. Similar to support vector machine (SVM), support vector regression (SVR) uses a linear kernel function for its regression. The difference with SVM, SVR also assigns a tolerance margin (ξ) to the estimate, apart from ε such as in SVM [40].

$$\min \frac{1}{2} \left\| w^2 \right\| + \sum_{i=1}^{n} \left(\xi_i + \xi_i^* \right)$$
$$s.t. : \begin{cases} z_i - (w \cdot \phi + b) & \leq \varepsilon + \xi_i \\ (w.\phi) + b - z_i & \leq \varepsilon + \xi_i^* \\ \xi_i \xi_i^* & \geq 0 \end{cases} \tag{12}$$

Optimization of the value will be done by determining the load, w subject to three optimization targets with z_i being the target line. The value will be used later for the decision limit to determine whether the leakage current has crossed the limit or not so that it can follow the previously discussed state representation. The digital part of this RCD will be attached directly to the medical device so that it can assist in electrical safety testing during maintenance [41]. Based on the results of testing and monitoring, the loading parameters will be periodically evaluated whether the condition of the device has changed or not. If the results show a change, the medical device needs to be scheduled for investigation before re-adjustment from machine learning on the server.

In addition, a server will be used for machine learning. As prediction of the machine's safety status could also be done using the LSTM method. The application of LSTM in the residual current signals could give more than just detection from current data as it is continuously fed by the digital RCD and recorded as historical data. Prediction based on the log is done using a time series pattern [22].

$$\begin{aligned} f(n) &= \sigma_g \left(W_f y(n) + U_f h(n-1) + b_f \right) \\ i(n) &= \sigma_g \left(W_i y(n) + U_i h(n-1) + b_i \right) \\ o(n) &= \sigma_g \left(W_o y(n) + U_o h(n-1) + b_o \right) \\ \tilde{c}(n) &= \sigma_c \left(W_c y(n) + U_c h(n-1) + b_c \right) \\ c(n) &= f(n) \odot c(n-1) + i(n) \odot \tilde{c}(n) \\ h(n) &= o(n) \odot \sigma_h \left(c(n) \right) \end{aligned} \tag{13}$$

Equation (13) shows the calculation of the output function and gate parameters used in the LSTM calculation. Respectively $f(n)$ is used for the forget gate, $i(n)$ for the input gate, and $o(n)$ for the output gate. As well as several activation functions, such as; σ_g for sigmoid, σ_c and σ_h are for the hyperbolic tangent. Several weights are also used, including; W for loading from the previous classification output, and U for loading from the LSTM recurrent cell that stores historical data that will be brought to the future prediction.

By simplifying the model above, it can produce faster results and fewer system parameters [42].

III. RESULTS AND DISCUSSION

Based on the design of the digital RCD, $t_{detection}$ could be based on the waveform pattern. Meanwhile, $t_{communication}$ can rely on the FO-based communication speed. Then, a broad view is directed back to $t_{coordination}$ as discussed before at (1). The approach of each time factor would be implemented in the digital RCD and with machine learning on the server. The design started from coordination with a model of residual current reading and the evaluation of the possible features for the detection in the digital RCD. Then, it was continued with the prediction model with its implementation using FPGA. Next, it was communication signals via FO utilizing the WDM technique and the prediction which could be from LSTM to speed up the overall time. Finally, it was discussed with a comparison with existing methods.

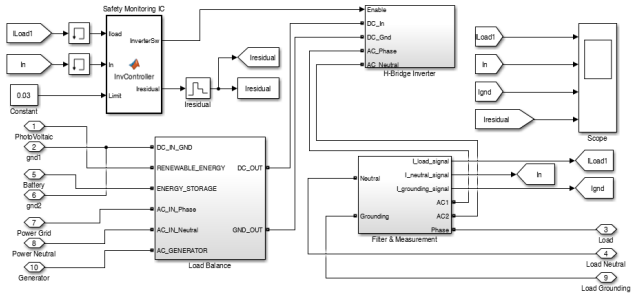

FIGURE 6. Microgrid control using residual current at server.

A. IMPLEMENTATION OF THE METHODS

Figure 6 shows the block diagram in the server section to realize the relationship between RCM and Inverter control as the most important part of the microgrid as previously discussed in its communication architecture via FO in Fig. 3. The basic idea of this block relationship is still the same with the presence of detection variations with coordinated medical equipment inputs to then be approached with supervised learning. The input will be divided into two groups. The first group can be done by simulating a full current loss as a single fault condition (SFC) and the second by recording data from normal conditions (NC) for training a specific medical device model. This medical device, like most electrical-based machines, will have unique characteristics for the large residual current value at (14).

$$\sum I_{\Delta} = \sum I_{Load} - \sum I_{Neutral} \tag{14}$$

I_{Load} and $I_{Neutral}$ are respectively being the incoming and outgoing currents in the medical device load then I_{Δ} is the residual current which will be read. It will be used to adjust the microgrid conditions seen in Fig. 1. Fig. 6 also utilizes resources from four sources: main grid, battery as energy backup, PV Array source, and DG for black start capability. Load Balance block will manage the proportion of power supply from each source according to its function [4].

Safety monitoring IC block will help to solve the operational characteristic equation in DOCR. By still utilizing the OCR index as is common in the relay sequence of the feeder line for protective coordination of the OCR in the trip time delay of the power distribution system [43]. The difference with this method is that the relay can also be activated by residual current based on the difference in (14). Analysis of the unsymmetrical ground fault or the symmetrical ground fault is done by confirming the proposed index. As shown previously in Fig. 2 with the example of CB329, CB330, and cable9, with the time delay arranged from bottom to top. Past values can be used to shorten the analysis of the coordination delay.

The lag model is a prediction concept using past data. This type of model is suitable for time series data as seen in the leakage current signal pattern. This model is commonly used with statistical data where present values are predicted by utilizing a regression equation based on previous values in one lagged period. The distributed lag model starts with an assumed structure with explanatory variables in (15).

$$y_k[n] = b + w_0x[n] + w_1x[n-1] + w_2x[n-2] + \ldots + w_nxn - k + \varepsilon \tag{15}$$

When x is the current input value and k is the period length, the predicted values y_k will be obtained. This Lag value will help form the LSTM model that will be made to accelerate the decision-making of leakage current detection by using validation within a specified time. Thus, the confirmation using an overall pattern with a long period can be shortened.

The data collection is carried out in the digital RCD as in Fig. 7. This pattern ensures the efficiency of data transmission in communication via FO between the digital RCD and the remote server. The feature of determining the length of the k value or the number of data samples from $x\,[n]$ until $x\,[n-k]$ will be evaluated later. This will also limit the tendency of the LSTM model to use forget gates, which can cause important information to be undetermined instead of fast speed [44].

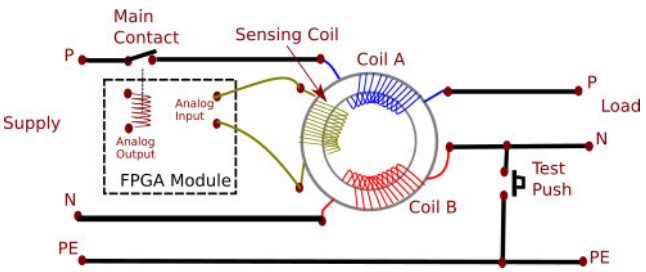

FIGURE 7. Digital RCD circuit at medical device load.

Figure 7 depicts how the RCD is connected to the FPGA which will be used for implementation. The module will be installed in each medical device that needs to be monitored and secured according to IEC standards. The circuit is also equipped with a push button that will simulate the conditions

of the SFC which will bypass the return current to the protective earth (PE) so that the LCC can be obtained. The data gathered from this circuit will be sampled and sent directly to the server to be processed with machine learning according to the relay coordination that has been discussed.

$$V_{RCD}(m,n) = \sum\sum(h_{Load}(k,l) * i_{\Delta}(m-k, n-l)) \tag{16}$$

$V_{RCD}(m,n)$ is the induction voltage used for relay coordination at each point m for residual current at sampling time n. The value will be classified using the SVR method before being processed on the server for further recording and processing. The value of the digital RCD is in accordance with the magnetic field induction physics formula as in (17).

$$V_{RCD} = -\frac{d\phi_B}{dt} \tag{17}$$

As there is a change in flux from the magnetic field ϕ_B over time, its value will be proportional to the current value through the RCD toroid. The single-phase source signal in the form of sin ωt changes in the form as shown in Fig. 4. However, with the characteristics of each load, the peak value and fluctuation value of the high-frequency pulse can change by stimulating the NC and SFC conditions. NC is the normal use of the device while SFC is a condition with leakage current [45]. Some features for each condition can be calculated which can then be implemented using FPGA module. Conditioning medical devices with two scenarios NC and SFC will produce different signals. In real conditions, the residual value i_{Δ} of leakage current can flow to PE, which will result in ground fault in its accumulation according to (14).

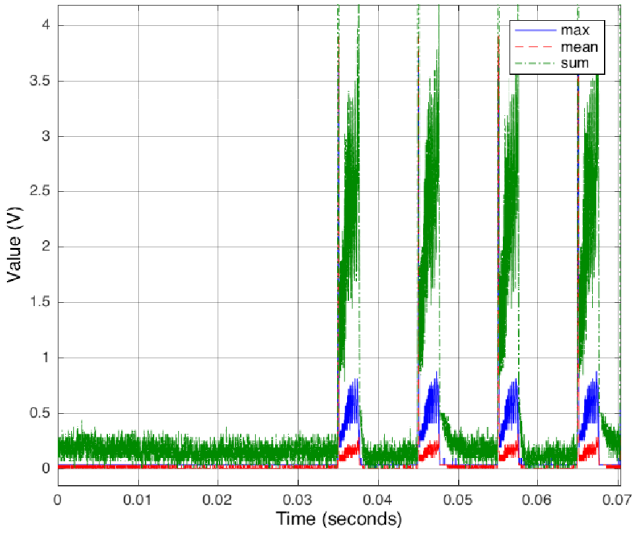

FIGURE 8. Features of sample data.

The signal in Fig. 4 with two hypothetical conditions that have been discussed will be used again to see the shape of its features in Fig. 8.

$$V_{Mean} \leq V_{Max} < V_{Sum} \tag{18}$$

Visually, it can be seen that there is a distance between the Max, Mean, and Sum features in each zone in Fig. 8. The output of each feature shows the average order from the smallest is Mean, Max, and Sum respectively. By emphasizing the difference in value of each zone between NC and LCC, the detection of leakage current analogously can be improved. Especially the L zone of each NC and LCC condition. Where it can be seen in Fig. 4, the L zone value is about the same in both conditions so using the raw value alone as a detection criterion would be risked by false detection.

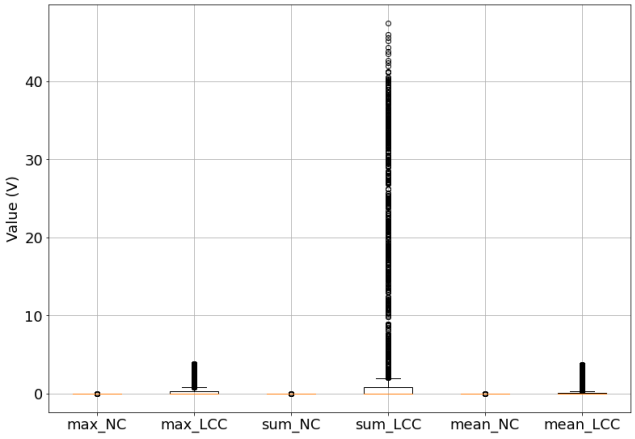

FIGURE 9. Distribution for each Feature.

To confirm the difference in values, a visualization of the distribution of values for each feature is performed in Fig. 9. It is specially to show the peak at the feature of Sum which was being cut to accommodate the waveform of other features in Fig. 8. Although the peak value of each feature shows the different values as in (18), the lower limit value does not give any difference. This is due to the existence of an almost identical L zone between the NC and LCC.

$$Spread_{Max} \leq Spread_{Mean} < Spread_{Sum} \tag{19}$$

Fig. 9 only shows the difference in the spread of each feature. This is because the value used in calculating the feature is the absolute value of the raw data with the same Minimum value at 0.0V and the Maximum value is 0.0314V and 3.8275V for both NC and LCC status respectively as shown in Fig. 4. This makes the comparison of the distribution only have a maximum value with a positive spread without any negative values. The comparison of the results between the features obtained shows a slight difference with (18) although the highest value still comes from the summation. The order of the spread values from the smallest is Max, Mean and Sum respectively. The Max and Mean values alternate in order to (19) with a spread distance between the two and a Sum of more than 40 points.

The difference in Sum value is needed to emphasize the threshold value or trip point on digital RCD but of course

it does not rule out the possibility that other features are also needed considering the relationship of the lag model. It should be noted that the tripping value is likely different from the commonly used analog RCD rating such as 30-mA. Which also generally has a limit of 80% of the tiered tripping value [28]. The determination of the trip value to be carried out is not affected by the value shift. This is because of the difference other than the tripping value which not only uses standard current measurements but also direct induction value readings from the data log. The tripping value error is a relatively larger part of the tripping value with machine learning.

Thus, the use of different period lengths to see further the differences of each feature. The existence of grouping using past values will make its value change according to the longer or shorter lag period. In other words, choosing the right latency length is important to get a mathematical correlation. However, choosing the length of the period is not easy. Especially for Data sets that have relationships that are difficult to identify. For that, the feature selection method with filters and wrappers can be applied [46]. However, this method also often eliminates elements that have nonlinear effects [44]. Following, the relationship between the length of the sampling period of the lag model and the average value in each feature is shown in Fig. 10.

$$Rate_{Mean} \leq Rate_{Max} < Rate_{Sum} \tag{20}$$

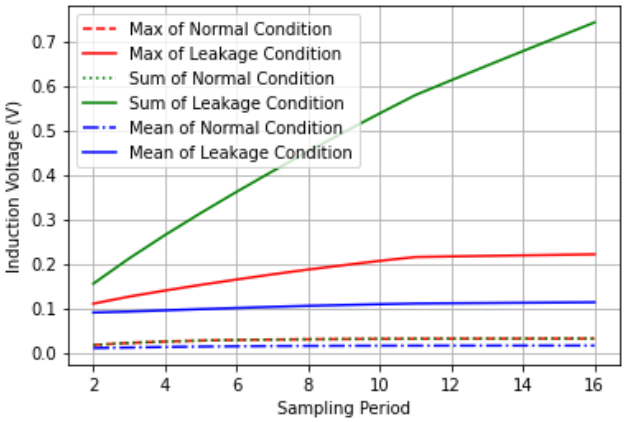

FIGURE 10. Average comparison between features.

As seen in Fig. 10, the comparison of the three features against the variation of sampling length shows a similar relationship to (18) during LCC. The Sum value is seen to be getting bigger with the highest rate followed by the Max and Mean values respectively. There is a tendency for the average value to be higher with the length of the sampling value with the rate sequence as in (20). This supports the necessary machine learning assistance in order to clarify its classification model over power supply characteristics.

Machine learning of these three features can help detect pattern stages when in LCC. However, with the reality of changes in value in each sampling length, the learning model needs to pay attention to the sampling length. On the other hand, the sampling length is also adjusted to the speed of the FPGA, in addition to determining the prediction model in (16). Finally, the search for the most optimal period length from both the hardware and software side might pay attention to the classification model target that matches (12).

B. CLASSIFICATION MODEL

Following the analysis of the results of the three previous features, the next target is to see its use in the weight of the prediction model. Before then implement it into a circuit in the Xilinx Spartan-6 FPGA. The circuit is generally built by utilizing the devices available in the HDL library, while still using the previously simulated simulation model. The FSM unit with CFG in Fig. 5 will use the three features that have been studied. Finally, the $t_{detection}$ time factor is determined by how the LCC pattern detection reaches the time required by IEC [7].

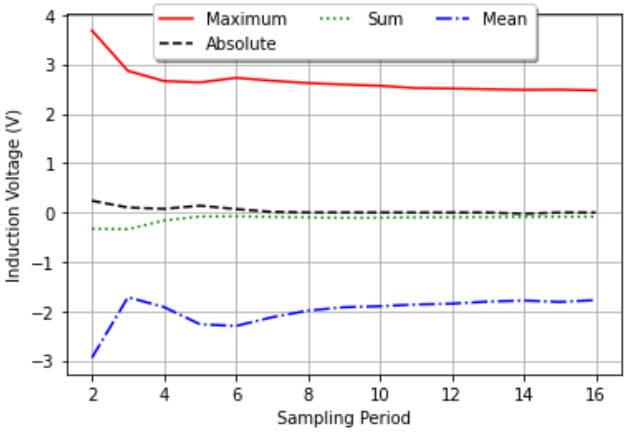

FIGURE 11. Weight value for possible different sampling.

Figure 11 shows the comparison of weight values for each sampling period length from 2 to 16. The value of each weight is obtained from the trained model of machine learning using the SVR method with the function in (22). The total data used is 70,324 in about 0.07 seconds as seen in the Signal Sample of RCD in Fig. 4. The comparison of the number of training data vs. test data is 70:30. The training process is carried out to obtain the value of the weight array W and the constant b as seen in (11). The graphic results show how much influence each weight has on Max, Mean, Sum and Absolute values. All operations can be compared again with the results of the previous value of each feature.

$$\mathcal{W} : \begin{cases} w_{Max} \cong w_{Mean}, \\ w_{Abs} \cong w_{Sum}. \end{cases} \tag{21}$$

The relationship of each weight shows the correlation of the two feature pairs in (21), between Max and Mean against the Absolute and Sum pairs. In theory, the machine learning model to be created will adjust the training data in a series

of transformations in the applied detection status learning. However, because here the pattern of the RCD function is used, the FSM will decide the final detection status of the suggestion value of the SVR classification. The linear function formed is represented by the feature transformation that has been previously analyzed in (11).

$$Y_{SVR} = W^T \begin{bmatrix} \phi_{Abs} \\ \phi_{Max} \\ \phi_{Sum} \\ \phi_{Mean} \end{bmatrix} + b \tag{22}$$

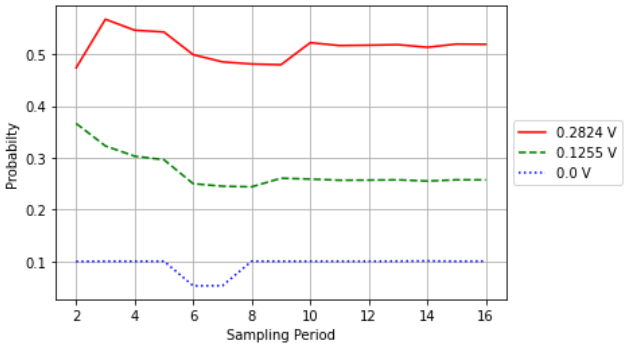

FIGURE 12. Probability with different sampling.

The result of the calculation in (22) can be seen in Fig. 12, which can be used as the probability value of LCC detection for three values of induction voltage, namely 0.0V, 0.1255V, and 0.2824V as a comparison. The three values show how with a difference of around 0.28 V it has reached an average of 50% probability of being detected as LCC regardless of the length of the sampling period. The value in NC is actually not large in value as shown in the distribution graph in Fig. 9. This is different from the distribution in LCC with a peak pattern in its H zone. The representation of the probability value could be calculated using a gradual transformation from the values convolution of Fig. 10 and Fig. 11.

The need to update the weight value of the classification model can basically also be used as a maintenance schedule based on changes or fault indications using the basic concept of corrective maintenance (CM) [47]. The implementation of this maintenance certainly also depends on the type of maintenance and the time interval that can be adjusted later with consideration of the large changes read from the RCD compared to the type of work required. The standardized matrix can also be used to compare the relative importance of each indication based on the assessment matrix with changes in the features read [48].

Maintenance will be scheduled with the indication of the $flag_{Maintenance}$ marked (1) which indicates the need for a maintenance schedule or unscheduled (0) as seen in Algorithm 1. The use of SVR will limit the permissible value of the induction voltage value read by the RCD, $V_{RCD}(m, n)$ within the tolerance margin ξ. With a rigid ξ value, CM can become condition-based maintenance (CBM). CBM is the use of condition monitoring to schedule maintenance before any faults happen and only by indication of them. It could increase the life of equipment with effectiveness on scheduled maintenance rather than regular preventive maintenance (PM) to ensure the safety of medical equipment.

Algorithm 1 also states that Weight changes occur with the condition of LCC detection because only that status has a

Algorithm 1 Algorithm for Updating the Weight Values

Input: Distributed Residual Current Values $V_{RCD}(m, n) = \sum\sum(h_{Load}(k, l) * i_{\Delta}(m - k, n - l))$

Output: New Weight Values for Digital RCD

Initialization:

W[n] = W[n-1]

Process Loop:

Check for possible LCC Pattern

if $(flag_{LCC})$ **then**

  Medical Device Relay Switched Off

  if $(\phi(V_{RCD}) \leq \phi_{Average} + \xi)$ **then**

    $flag_{Maintenance} = 0$

  else

    $flag_{Maintenance} = 1$

    Run SVR to get new Weight Values at Server

  end if

end if

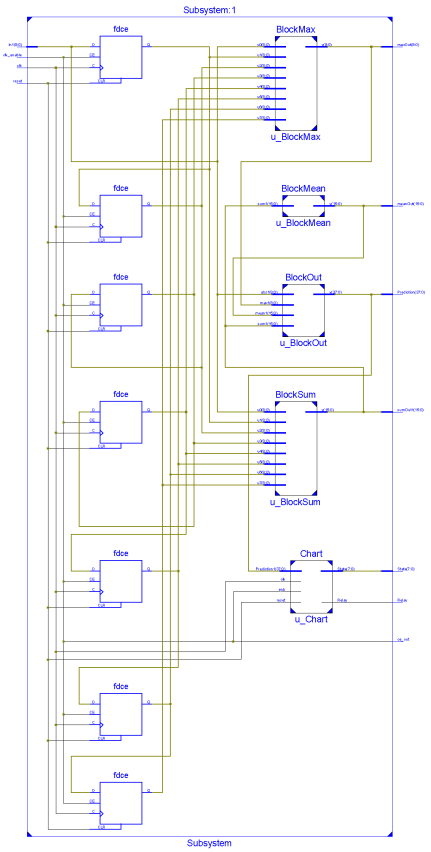

FIGURE 13. RTL of FPGA schematic design with period length of 7.

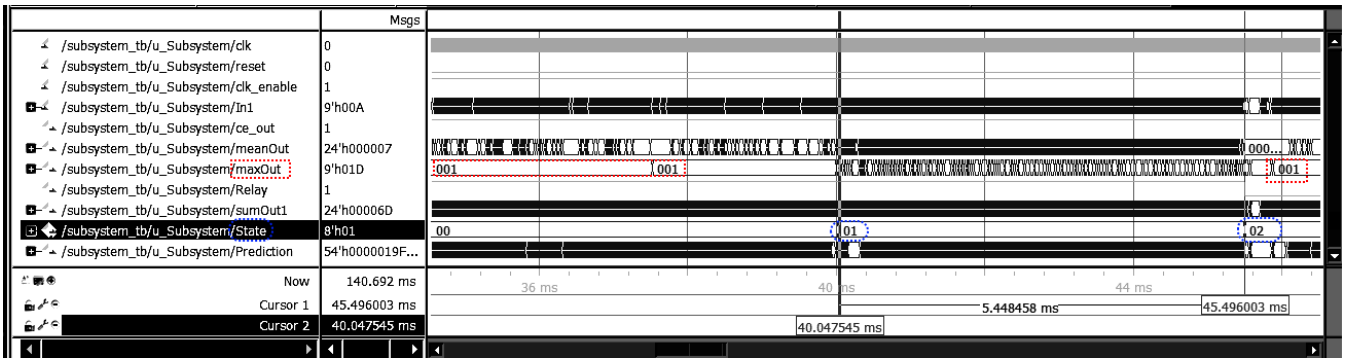

FIGURE 14. Timing diagram.

peak value. The value where the magnitude can exceed the tolerance limit. The implementation of LCC detection will be realized using FPGA as shown in Fig. 13. The module is part of the digital RCD that has been discussed in Fig. 7. It is also used for decision makers for any relay's trip once LCC is detected at the attached loads.

Figure 13 shows the Register-Transfer Level (RTL) design with a Period Length of 7. Three features would be synthesized in hardware and fed into the target FPGA core, namely; Max, Mean and Sum. According to the concept of the lag model, these features would be calculated using the past values collection. The feature calculation was designed in each block, which was in *BlockMax*, *BlockMean*, and *BlockSum* with signal output names of *maxOut*, *meanOut*, and *sumOut*1 respectively shown in Fig. 14. With simple arithmetic operations at the RTL level, the value of each past value was stored in a memory cell by following the period length from the lag model. Furthermore, a versatile and customizable CPU core could be utilized so that we can improve it. For example, it could use a CPU architecture that also has digital communication features such as RISC-V so it would be more accurate [49]. However, this design had been built using fixed points so that it could be fast in processing the detection while keeping efficiency in the implementation of the design model [50].

Figure 14 shows the timing diagram results of the time simulation for each signal in Fig. 13. With the pattern detection of the waveform signal in the CFG that has been discussed in Fig 5, it could be seen that the time needed from state 1 to state 2, circled in blue color took only about 5.45ms which shown with the inverted color of signal name, State. This interval value was the length of the H to L signal detection in the LCC, which was confirmed also with a low value at the signal name of *maxOut* at h001, circled in red color during both states 0 and 2. The time length was shorter than the half of T length at 10ms using (6). Timing diagram simulation was needed to ensure that there was only not much difference in the result between the use of the HDL library and the model simulation in Matlab. As a comparison, Fig 5 visually shows that the period H is about 3.10ms. In addition to the timing diagram, we could also see how efficiently the FPGA resources were used in Table 3.

TABLE 3. FPGA map report.

Slice Logic Utilization	Used	Available	Utilization
Number of Slice Registers	184	18,224	1%
Number of Slice LUTs	1,656	9,112	18%
Number of occupied Slices	505	2,278	22%
Number of MUXCYs used	796	4,556	17%

Table 3 shows how many resources were used to realize the FPGA module for the digital RCD. The final report includes the number of lookup tables (LUT), slice registers, and number of total employed slices. The FPGA hardware used was Xilinx based on XC6SLX16-2FTG256C, Spartan-6 Core with a clock frequency of 50MHz. It can be seen that the hardware design was quite simple using only 1% of the register capacity in the module. However, the focus of this module was to ensure patient safety. With the time difference between the FPGA simulation and Matlab being about 2.35ms, the detection time tolerance must take this into account. For comparison, 10ms was the required time for the let-go time for a current of 200mA in Table 2. The signal waveform had been fully detected from state 0 to 2 in Fig. 5. The pattern sequence of the LCC would be used to ensure that there was no false detection or nuisance trip while still ensuring the IEC standard. On the other hand, the value of features formed by the induced voltage from the RCD can vary as in Fig. 8. Therefore, machine learning is necessary in order to get updated values to form the pattern flow so it could work with its arbitrary form to get the detection [39].

C. RCM ACCELERATION

Acceleration here offers a cost-effective solution by reducing the need for extensive cabling and infrastructure [51]. Its compatibility with existing systems ensures seamless integration, providing a pathway for early detection of medical devices. Its implementation can foster greater trust and improve overall electrical safety standards. In addition to improving signal integrity, the use of FO also reduces susceptibility to electromagnetic interference. Enhanced data analysis capabilities enable proactive maintenance and real-time decision-making with CBM. The ability to analyze residual current data faster can help identify potential safety

TABLE 4. OSA points value.

Point	Power (dBm)	Wavelength (nm)
A	-88.79	1549.39
B	-81.34	1550.31
C	-73.88	1551.06

hazards. Not only does this proactive approach minimize communication time, but it also reduces detection time with LSTM-based predictions, which will be discussed later. The system can support the integrity of microgrid protection in meeting safety standards by improving timely accuracy.

The next problem is the acceleration from the communication side, $t_{communication}$ while ensuring that RCM remains effective with minimal noise. The use of FO with WDM will improve the integrity of various lights originating from many digital RCDs. This method realizes the transmission of several signals at once so that overall it can improve system performance and simplify maintenance. In the use of WDM allows the utilization of large bandwidth to facilitate the processing and analysis of each data, it is necessary to pay attention to the problem of crosstalk noise. This is important to be detected early so that there are no anomalies and can improve the reliability of the monitoring system. The design of this system also emphasizes scalability and allows for the expansion of the monitoring network [29].

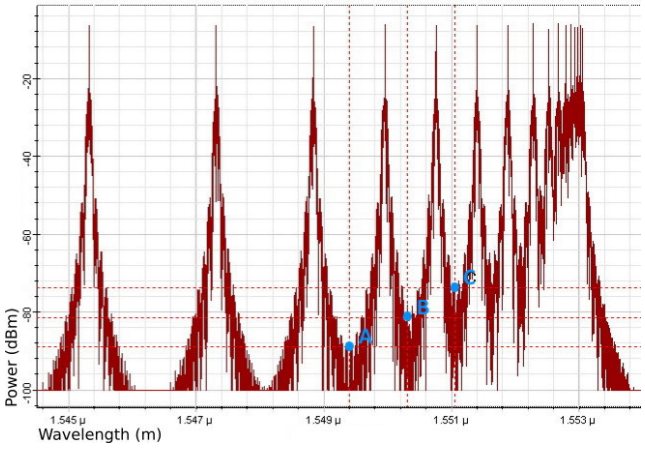

FIGURE 15. WDM signal at OSA.

The distribution of light signals using WDM needs to pay attention to the wavelength distance used. This is as seen in Fig. 15. The closer the distance, the greater the noise caused by the possible intersection of the light wavelength distribution. The average signal distribution is around 1.5nm which can be observed from the 2nd and 3rd signals from the left with center wavelengths of around 1548.9 and 1547.4 nm respectively. Thus, the difference in wavelength less than that will experience an intersection with the signal distribution from neighboring channels. In general, the signal will result in a not-too-high SNR with the presence of inter-channel crosstalk noise. The increasing noise level can be seen at represented points A, B, and C in Fig. 15. The details of the values are in Table 4.

TABLE 5. LSTM parameter.

Parameter	Value
Training Data Length	47,117
Testing Data Length	23,207
Training RMSE Score	0.71 %
Testing RMSE Score	1.09 %

Table 4 shows the noise value at each point A, B, and C. With the highest being point C, this value would be higher with the distance of the wavelength used getting shorter. With these three points, the distance between points could be obtained, which is 0.92 and 0.75 nm for each A-B and B-C respectively. While the difference in value is the noise level of −100 dBm was 11.21, 18.66, and 26.12 dBm for points A, B, and C. These values were highly dependent on the MUX filter's bandwidth, and power depth. The depth would have the greatest impact on the power level in each channel. In WDM systems, reducing channel crosstalk was essential to prevent problems with wavelength tuning later on.

Furthermore, detection speed acceleration could also utilize machine learning to predict. This allows for significant improvement in decision-making time to prioritize electrical safety. By utilizing LSTM, prediction of detection status can be done without having to wait for the full wave period. RCD signal would repeat twice in a period, T on its absolute value signal which could be compared with Fig. 4. It could be detected with only one and a half of the H-L pattern. This would shorten the time from what it should be at 20ms for one full period in RCD. It might take around 15ms depending on the H-L detection speed from FPGA with the possibility of error that corresponds to the LSTM model testing as seen in Fig. 16. Using this pattern evaluation, the RCD was no longer sensitive due to surges in impulse values which can be caused by supply voltage disturbances or current surges which magnified by the electronic loads and discharge to ground [8].

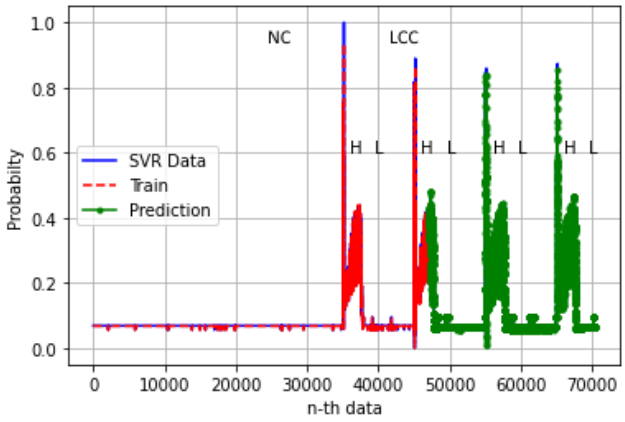

FIGURE 16. Prediction using LSTM cf. Fig. 4.

Fig. 16 shows the training and testing results of the probability signal from the SVR results in Fig. 12. The pattern generated from the previous classification with its absolute voltage value with the previous range of 0 to 4 in Fig. 4,

TABLE 6. Category of fault condition monitoring method.

Target	Wave form	State Trans.	Weight Chng.
Utility Equipment Condition Monitoring [52]	V	-	-
The Calibration of Medical Testing Equipment [39]	V	-	-
Health Assessment for Electronic Components [53]	-	V	-
CBM for Transmission and Transformation Equipment [48]	-	-	V
Proposed RCM	V	V	V

had been changed to a probability value of 0 to 1 after data normalization in Fig. 16. The test and training results conditions can be seen at Table 5. The comparison of the length of the training and testing data was 47,117 vs. 23,207. From the testing results, the root mean square error (RMSE) value was around 1 % for each of the training and testing. The difference in value can be seen in the Peak Value between SVR Data vs. prediction in each group, both from training and testing in Fig. 16. With a small RMSE value, the signal's waveform can certainly still be read from the prediction value and the results can be used to speed up detection. In other words, confirmation of LCC detection is more towards the H-L-H pattern with a possible 3/4 of the full wave. As the full period of the AC signal consisted of two absolute waves so detection might take within 15.45ms with an extra 10 ms from the half period using the FPGA speed as discussed in Fig. 14.

D. DISCUSSION

From the discussion of previous sections, it could be observed that there is more than one method used in building the proposed RCM system. These methods basically have been also used in other research based on fault monitoring. The following is a grouping per category of each method used in Table 6.

Table 6 provides a comparison of the proposed RCM method with other works in terms of its category. The use of each category is part of the entire system whereas, in this design system, Waveform is used in Digital RCD implemented in the FPGA module. As a comparison, [52] uses it to detect its abnormality [52] while [39] applies it with a sampling comparison. This can also be seen in how the comparison of results is done with different sampling lengths as Fig. 10 - 12. The state transition category which is seen in [53] is also applied to the waveform pattern sequence in Fig. 5. Furthermore, changes in the waveform of new application scenarios with different load types may be reflected in the SVR classification probability as it should be learned from the data when performing maintenance that will have weight calculations. Finally, the weight change that has been suggested in [48] has also been applied to Algorithm 1, which will respond when an LCC pattern is detected and the value obtained exceeds the tolerance threshold, ξ. In the case when many power electronic loads are present, a certain leakage current might be generated during NC. The SVR classification and LSTM normalization should be adjusted to the value so that the operating error could be minimized by the weights. Thus, the detection sensitivity would also depend on the tolerance given by the technician who performed the maintenance.

Overall, the combination of detection with the SVR method will be accelerated by the use of FO as a communication medium. Then, LSTM was used to predict from probability given by SVR for decision making at microgrid protection systems that are commonly applied with relay coordination. Therefore, LSTM should be used with pattern detection obtained from previous SVR classification. H-L-H pattern can be used to ensure that the detection is on target as predicted and the relay will be localized around the leakage current cause only.

This work attempts to develop a fast and adaptive detection mechanism, which is also suggested by [52]. Weight determination by machine learning has also been discussed to schedule maintenance as in [48]. This integrated RCM as a whole system will be updated continuously by the digital RCD as input and utilize the FO network with the proposed detection to control the microgrid. Then, it will make the microgrid overcome potential safety risks and keep it efficient by actively disconnecting potential sources of leakage current after confirmation. In other words, to improve electrical safety, this RCM design will support the existing microgrid protection system by giving information about any leakage current fault. More researches are needed for this patient safety using other detection methods, which could improve this FO-based system, such as a way of processing and computing using light directly without converting back to electrical voltage.

IV. CONCLUSION

Three components of protection time in microgrid system have been carried out in order to add patient safety as one of the fault parameters. The first was the detection time while avoiding false alarms. This could use a pattern sequence of RCD signal's waveform. Then, improvements in both communication and coordination were designed by using FO with WDM technique as the acceleration of previous pattern detection. This method also needed to be planned by considering the wavelength distance between its channels. Pattern detection of RCD voltage induction was realized by using FPGA module. Once a LCC occurs, FPGA would classify it with SVR method before performing protection. Then, a signal transmission with FO will bring novelty to speed up the fault analysis and protection in a microgrid. The signal would also be forwarded to the server for coordination process and accelerating detection also by using LSTM. The error value of RMSE when the server performs prediction test could be used as a judgment for microgrid controller in performing protection in its distribution management. This proposed system was designed using FO for data communication and relay coordination in microgrid. For

future projects, further use of FO for its direct data processing using light could be tested.

ACKNOWLEDGMENT

It was carried out to fulfill a Ph.D. degree by Research Study at the Department of Electrical Engineering, Faculty of Intelligent Electrical and Informatics Technology, Institut Teknologi Sepuluh Nopember. The testing was facilitated at the Photonics Laboratory, Department of Physics, Faculty of Science and Technology, Universitas Airlangga.

REFERENCES

[1] G. Parise, L. Parise, M. Allegri, A. D. Marco, and M. A. Anthony, "Operational resilience of hospital power systems in the digital age," *IEEE Trans. Ind. Appl.*, vol. 57, no. 1, pp. 94–100, Jan. 2021.

[2] S. A. Hosseini, S. H. H. Sadeghi, and A. Nasiri, "Decentralized adaptive protection coordination based on agents social activities for microgrids with topological and operational uncertainties," *IEEE Trans. Ind. Appl.*, vol. 57, no. 1, pp. 702–713, Jan. 2021.

[3] M. M. Alam, M. Shahjalal, M. H. Rahman, H. Nurcahyanto, A. T. Prihatno, Y. Kim, and Y. M. Jang, "An energy and leakage current monitoring system for abnormality detection in electrical appliances," *Sci. Rep.*, vol. 12, no. 1, p. 18520, Nov. 2022.

[4] E. Sutanto, F. Fahmi, Y. Nurdin, P. Puspitaningayu, and M. Aziz, "Microgrid monitoring for patient safety in hospital using distributed residual current," *IEEE Internet Things J.*, vol. 11, no. 18, pp. 29979–29992, Sep. 2024.

[5] A. Jain, O. Saborio-Romano, J. N. Sakamuri, and N. A. Cutululis, "Virtual resistance control for sequential green-start of offshore wind power plants," *IEEE Trans. Sustain. Energy*, vol. 13, no. 3, pp. 1420–1429, Jul. 2022.

[6] L. Silvestri, Y. Chen, Z. Brodzeli, T. Sirojan, S. Lu, Z. Liu, T. Phung, and F. Ladouceur, "A novel optical sensing technology for monitoring voltage and current of overhead power lines," *IEEE Sensors J.*, vol. 21, no. 23, pp. 26699–26707, Dec. 2021.

[7] *Low-Voltage Electrical Installations—Part 4–41: Protection for Safety—Protection Against Electric Shock*, Standard IEC 60364-4-41, 2005. [Online]. Available: https://standards.iteh.ai/catalog/standards/iec/66d2090a-8b47-43dc-bb2f-833f3a8cc8d0/iec-60364-4-41-2005

[8] G. Escrivá-Escrivá, C. R. Porta, and E. C. W. de Jong, "Nuisance tripping of residual current circuit breakers in circuits supplying electronic loads," *Electric Power Syst. Res.*, vol. 131, pp. 139–146, Feb. 2016.

[9] A. Gao and D. Zeng, "A novel concept of artificial intelligence utilization in electrical safety intelligent management system," in *Proc. 9th Int. Conf. Fire Sci. Fire Protection Eng. (ICFSFPE)*, Oct. 2019, pp. 1–4.

[10] S. Wang and P. Dehghanian, "On the use of artificial intelligence for high impedance fault detection and electrical safety," *IEEE Trans. Ind. Appl.*, vol. 56, no. 6, pp. 7208–7216, Nov. 2020.

[11] M. Doherty and B. Esmaeili, "Application of artificial intelligence in electrical safety," in *Proc. IEEE IAS Electr. Saf. Workshop (ESW)*, Mar. 2020, pp. 1–6.

[12] M. Khaleel, S. A. Abulifa, and A. A. Abulifa, "Artificial intelligent techniques for identifying the cause of disturbances in the power grid," *Brilliance, Res. Artif. Intell.*, vol. 3, no. 1, pp. 19–31, Mar. 2023.

[13] A. Iaccarino, C. G. Poyatos, F. Chiovoloni, N. G. Gómez, S. d'Angelo, and J. Petruzzi, "How disruptive artificial intelligence solutions can enhance safety of field operations in the electrical sector," in *Proc. 27th Int. Conf. Electr. Distrib.*, vol. 2023, no. 6, 2023, pp. 2039–2043, doi: 10.1049/icp.2023.1158.

[14] J. Wei, A. Chammam, J. Feng, A. Alshammari, K. Tehranian, N. Innab, W. Deebani, and M. Shutaywi, "Power system monitoring for electrical disturbances in wide network using machine learning," *Sustain. Comput., Informat. Syst.*, vol. 42, Apr. 2024, Art. no. 100959.

[15] L. Qi, X. Wei, W. Zhu, J. Zhou, and Y. Cao, "A failure detection method based on SVM model for solar power generation equipment," in *Proc. 10th Int. Symp. Syst. Secur., Saf., Rel. (ISSSR)*, Mar. 2024, pp. 495–501.

[16] D. Venu, "Design analysis and classification of digital transmission based composite relay and artificial neural network approach," *IJFANS Int. J. Food Nutritional Sci.*, vol. 12, no. 1, pp. 63–680, 2023.

[17] W. Chen, D. Subramanian, and S. Paternain, "Probabilistic constraint for safety-critical reinforcement learning," *IEEE Trans. Autom. Control*, vol. 69, no. 10, pp. 6789–6804, Oct. 2024.

[18] Y. Ye, H. Wang, P. Chen, Y. Tang, and G. Strbac, "Safe deep reinforcement learning for microgrid energy management in distribution networks with leveraged spatial–temporal perception," *IEEE Trans. Smart Grid*, vol. 14, no. 5, pp. 3759–3775, Sep. 2023.

[19] F. Möller, A. M. Blanco, and J. Meyer, "Characteristic leakage current of household devices and their impact on the tripping behaviour of residual current devices," *Electric Power Syst. Res.*, vol. 214, Jan. 2023, Art. no. 108832.

[20] T. Biswal and S. K. Parida, "A novel high impedance fault detection in the micro-grid system by the summation of accumulated difference of residual voltage method and fault event classification using discrete wavelet transforms and a decision tree approach," *Electric Power Syst. Res.*, vol. 209, Aug. 2022, Art. no. 108042.

[21] B. Wang, Z. Li, Z. Bai, P. T. Krein, and H. Ma, "A voltage vector residual estimation method based on current path tracking for T-Type inverter open-circuit fault diagnosis," *IEEE Trans. Power Electron.*, vol. 36, no. 12, pp. 13460–13477, Dec. 2021.

[22] A. Mohammad-Alikhani, B. Nahid-Mobarakeh, and M.-F. Hsieh, "One-dimensional LSTM-regulated deep residual network for data-driven fault detection in electric machines," *IEEE Trans. Ind. Electron.*, vol. 71, no. 3, pp. 3083–3092, Mar. 2023.

[23] W. Lang, Y. Hu, Z. Zhang, C. Gan, J. Si, and H. Wen, "Few-shot learning with residual current for EV inverter fault diagnosis of EV powertrain," *IEEE Trans. Transport. Electrific.*, early access, Jan. 12, 2024, doi: 10.1109/TTE.2024.3349619.

[24] Y. Zhou and C. Ngai-Man Ho, "A review on microgrid architectures and control methods," in *Proc. IEEE 8th Int. Power Electron. Motion Control Conf. (IPEMC-ECCE Asia)*, May 2016, pp. 3149–3156.

[25] T. S. Ustun, C. Ozansoy, and A. Zayegh, "Modeling of a centralized microgrid protection system and distributed energy resources according to IEC 61850–7–420," *IEEE Trans. Power Syst.*, vol. 27, no. 3, pp. 1560–1567, Aug. 2012.

[26] D. Birla, R. P. Maheshwari, and H. O. Gupta, "A new nonlinear directional overcurrent relay coordination technique, and banes and boons of near-end faults based approach," *IEEE Trans. Power Del.*, vol. 21, no. 3, pp. 1176–1182, Jul. 2006.

[27] S. P. Ramli, H. Mokhlis, W. R. Wong, M. A. Muhammad, and N. N. Mansor, "Optimal coordination of directional overcurrent relay based on combination of firefly algorithm and linear programming," *Ain Shams Eng. J.*, vol. 13, no. 6, Nov. 2022, Art. no. 101777.

[28] K. Li, J. Lin, F. Niu, Y. Wang, Q. Li, Z. Guo, and Y. Wu, "A novel fault leakage current detection method with protection deadzone elimination," *IEEE Trans. Instrum. Meas.*, vol. 70, pp. 1–9, 2021.

[29] E. Sutanto, G. Escrivá-Escrivá, H. Kusuma, and T. A. Sardjono, "Efficient FO-based WDM-PON communication model of residual current monitoring for medical devices," in *Proc. 29th Int. Conf. Telecommun. (ICT)*, Nov. 2023, pp. 1–6.

[30] A. Totovic, G. Giamougiannis, A. Tsakyridis, D. Lazovsky, and N. Pleros, "Programmable photonic neural networks combining WDM with coherent linear optics," *Sci. Rep.*, vol. 12, no. 1, p. 5605, Apr. 2022.

[31] N. Singh, "Application of fiber optics for the protection and control of power systems," in *Optical to Terahertz Engineering* (Progress in Optical Science and Photonics). Singapore: Springer, 2023, pp. 101–120. [Online]. Available: https://link.springer.com/chapter/10.1007/978-981-99-0228-6_7#citeas

[32] *Effects of Current on Human Beings and Livestock—Part 1: General Aspects*, IEC/TS 60479-1, 2018.

[33] I. E. Commission, *Medical Electrical Equipment—Part 1: General Requirements for Safety and Essential Performance*, Standard IEC 60601-1, 1995.

[34] T. Penthong, M. Ginocchi, A. Ahmadifar, F. Ponci, and A. Monti, "IEC 61850-based protection scheme for multiple feeder faults and hardware-in-the-loop platform for interoperability testing," *IEEE Access*, vol. 11, pp. 65181–65196, 2023.

[35] D. Jain and B. Iyer, "Design and analysis of high-speed four-channel WDM radio over fiber system for millimeter-wave applications," *Int. J. Syst. Assurance Eng. Manage.*, vol. 14, pp. 746–758, Jul. 2023.

[36] R. Sharma and A. Sharma, "IS OWC WDM system performance optimization at 40 Gbps bit rate with improved link distance of 10000 km," in *Proc. Int. Conf. Inventive Res. Comput. Appl. (ICIRCA)*, Jul. 2018, pp. 795–799.

[37] M. S. Goodman, H. Kobrinski, M. P. Vecchi, R. M. Bulley, and J. L. Gimlett, "The LAMBDANET multiwavelength network: Architecture, applications, and demonstrations," *IEEE J. Sel. Areas Commun.*, vol. 8, no. 6, pp. 995–1004, Aug. 1990.
[38] E. Sutanto, "Sample of RCD (residual current device) induction voltage," *IEEE Dataport*, Oct. 2024, doi: 10.21227/th4z-x215.
[39] S. S. L. Yang, B. H. S. Lam, and C. M. N. Ng, "Digital sampling technique in the calibration of medical testing equipment with arbitrary waveforms," in *Proc. IEEE Int. Symp. Med. Meas. Appl. (MeMeA)*, Jun. 2018, pp. 1–6.
[40] S. Kavitha, S. Varuna, and R. Ramya, "A comparative analysis on linear regression and support vector regression," in *Proc. Online Int. Conf. Green Eng. Technol. (IC-GET)*, Nov. 2016, pp. 1–5.
[41] N. Piotrowski, "Future trends of electrical safety testing—Production electrical safety testing," in *Proc. IEEE Symp. Product Compliance Eng. (ISPCE)*, May 2016, pp. 1–4.
[42] H. Çimen, N. Çetinkaya, J. C. Vasquez, and J. M. Guerrero, "A microgrid energy management system based on non-intrusive load monitoring via multitask learning," *IEEE Trans. Smart Grid*, vol. 12, no. 2, pp. 977–987, Mar. 2021.
[43] Y. J. Cho and S.-H. Lim, "Analysis on protection coordination of OCRs using index for impedance compensation considering unsymmetrical ground fault in a power distribution system with SFCL," *IEEE Trans. Appl. Supercond.*, vol. 33, no. 5, pp. 1–6, Aug. 2023.
[44] F. Martinez-Garcia and D. Down, "E-LSTM: An extension to the LSTM architecture for incorporating long lag dependencies," in *Proc. Int. Joint Conf. Neural Netw. (IJCNN)*, Jul. 2022, pp. 1–8.
[45] E. Sutanto, K. Ain, M. Aziz, and G. Escrivá, "A study on DC limit parameters in RCD operation using capacitor," *J. Eng. Sci. Technol. Rev.*, vol. 12, no. 4, pp. 7–14, Aug. 2019.
[46] H.-H. Hsu, C.-W. Hsieh, and M.-D. Lu, "Hybrid feature selection by combining filters and wrappers," *Exp. Syst. Appl.*, vol. 38, no. 7, pp. 8144–8150, Jul. 2011.
[47] N. H. A. Rahman, K. Hasikin, N. A. A. Razak, A. K. Al-Ani, D. J. S. Anni, and P. Mohandas, "Medical device failure predictions through AI-driven analysis of multimodal maintenance records," *IEEE Access*, vol. 11, pp. 93160–93179, 2023.
[48] H. Wang, D. Lin, J. Qiu, L. Ao, Z. Du, and B. He, "Research on multiobjective group decision-making in condition-based maintenance for transmission and transformation equipment based on D-S evidence theory," *IEEE Trans. Smart Grid*, vol. 6, no. 2, pp. 1035–1045, Mar. 2015.
[49] M. Tourres, C. Chavet, B. Le Gal, J. Crenne, and P. Coussy, "Extended RISC-V hardware architecture for future digital communication systems," in *Proc. IEEE 4th 5G World Forum (5GWF)*, Oct. 2021, pp. 224–229.
[50] A. Giorgio, "Project and implementation of a quantum logic gate emulator on FPGA using a model-based design approach," *IEEE Access*, vol. 12, pp. 41317–41353, 2024.
[51] F. Rühl and T. Anderson, "Cost-effective metro WDM network architectures," in *Opt. Fiber Commun. Conf. Exhib. Tech. Dig.*, vol. 3, 2001, p. WL1.
[52] B. Li, Y. Jing, and W. Xu, "A generic waveform abnormality detection method for utility equipment condition monitoring," *IEEE Trans. Power Del.*, vol. 32, no. 1, pp. 162–171, Feb. 2017.
[53] S. Zhao, V. Makis, S. Chen, and Y. Li, "Health assessment method for electronic components subject to condition monitoring and hard failure," *IEEE Trans. Instrum. Meas.*, vol. 68, no. 1, pp. 138–150, Jan. 2019.

ERWIN SUTANTO (Graduate Student Member, IEEE) received the B.Sc. degree in electronics from Institut Teknologi Bandung (ITB), in 2002, and the M.Sc. degree in IC design (electronics) from Nanyang Technological University (NTU), Singapore, in 2008. He is currently pursuing the Ph.D. degree with the Department of Electrical Engineering, Faculty of Intelligent Electrical and Informatics Technology, Institut Teknologi Sepuluh Nopember (ITS). After working for a few years in various industries, he joined Universitas Airlangga as a Lecturer, in 2016. His research interests include digital circuits, electromagnetic, android programming, fiber optics, and its applications in medical safety devices.

GUILLERMO ESCRIVÁ-ESCRIVÁ received the Ph.D. degree in industrial engineering from Universitat Politècnica de València (UPV), in 2009. He has been a Professor with the Electrical Engineering Department, UPV, since 2005. From 2000 to 2005, he worked at the significance construction company as the Facility Manager. His research work is developed at the Institute for Energy Engineering and includes studies about renewable energy resources management, energy efficiency, power quality, and power markets. He presents a high technical training in research and applied studies and great interest in the transfer of knowledge from the university to the industry and vice versa.

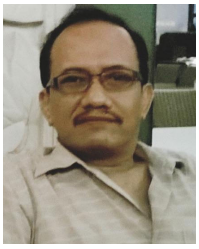

SAMIAN SAMIAN received the bachelor's degree in physics from Universitas Airlangga, Indonesia, in 1996, and the master's degree from Institut Teknologi Sepuluh Nopember, Indonesia, in 2008. He is currently an Associate Professor with the Photonics Laboratory, Universitas Airlangga, Indonesia. His research interest includes fiber sensors.

HENDRA KUSUMA (Member, IEEE) received the B.S. degree in electrical engineering from Institut Teknologi Sepuluh Nopember, Surabaya, in 1988, the M.S. degree in renewable energy engineering from the Curtin University of Technology, in 2001, and the Ph.D. degree in electrical engineering from Institut Teknologi Sepuluh Nopember, in 2016. Since 1989, he has been a Lecturer with the Department of Electrical Engineering, Institut Teknologi Sepuluh Nopember. He is currently the Head of the Microelectronic and Embedded System Laboratory, Department of Electrical Engineering, ITS. His research interests include artificial intelligence, machine learning, pattern recognition, power electronics, the IoT, and assistive technology.

TRI ARIEF SARDJONO (Member, IEEE) was born in Surabaya, in February 1970. He received the bachelor's degree in electrical engineering from Institut Teknologi Sepuluh Nopember, Surabaya, Indonesia, in 1994, the master's degree in biomedical engineering from Institut Teknologi Bandung, Indonesia, in 1996, with a focus on health management information systems for community health centers, and the Ph.D. degree from the University of Groningen/University Medical Center Groningen, in September 2007. Since 1995, he has been with the Electrical Engineering Department and the Biomedical Engineering Department, Institut Teknologi Sepuluh Nopember, in 2015. His research interest includes medical image processing and analysis.